

# Mesoscale Dynamics and Its Application in Torrential Rainfall Systems in China

GAO Shouting<sup>\*1</sup>, TAN Zhemin<sup>2</sup>, ZHAO Sixiong<sup>1</sup>, LUO Zhexian<sup>3</sup>, LU Hancheng<sup>4</sup>,  
WANG Donghai<sup>5</sup>, CUI Chunguang<sup>6</sup>, CUI Xiaopeng<sup>1</sup>, and SUN Jianhua<sup>1</sup>

<sup>1</sup>*Laboratory of Cloud-precipitation Physics and Severe Storms, Institute of Atmospheric Physics,  
Chinese Academy of Sciences, Beijing 100029*

<sup>2</sup>*Department of Atmospheric Sciences, Nanjing University, Nanjing 210093*

<sup>3</sup>*Remote Sensing College, Nanjing University of Information Science & Technology, Nanjing 210044*

<sup>4</sup>*Meteorological College, PLA University of Science and Technology, Nanjing 211101*

<sup>5</sup>*Chinese Academy of Meteorological Sciences, Beijing 1000081*

<sup>6</sup>*Institute of Heavy Rain, China Meteorological Administration, Wuhan 430074*

(Received 20 May 2014; revised 1 July 2014; accepted 30 July 2014)

## ABSTRACT

Progress over the past decade in understanding moisture-driven dynamics and torrential rain storms in China is reviewed in this paper. First, advances in incorporating moisture effects more realistically into theory are described, including the development of a new parameter, generalized moist potential vorticity (GMPV) and an improved moist ageostrophic  $\mathbf{Q}$  vector ( $\mathbf{Q}_{um}$ ). Advances in vorticity dynamics are also described, including the adoption of a “parcel dynamic” approach to investigate the development of the vertical vorticity of an air parcel; a novel theory of slantwise vorticity development, proposed because vorticity develops easily near steep isentropic surfaces; and the development of the convective vorticity vector (CVV) as an effective new tool. The significant progress in both frontal dynamics and wave dynamics is also summarized, including the geostrophic adjustment of initial unbalanced flow and the dual role of boundary layer friction in frontogenesis, as well as the interaction between topography and fronts, which indicate that topographic perturbations alter both frontogenesis and frontal structure. For atmospheric vortices, mixed wave/vortex dynamics has been extended to explain the propagation of spiral rainbands and the development of dynamical instability in tropical cyclones. Finally, we review wave and basic flow interaction in torrential rainfall, for which it was necessary to extend existing theory from large-scale flows to mesoscale fields, enriching our knowledge of mesoscale atmospheric dynamics.

**Key words:** mesoscale dynamics, torrential rainfall, moist atmosphere, vorticity dynamics, wave-flow interaction

**Citation:** Gao, S. T., and Coauthors, 2015: Mesoscale dynamics and its application in torrential rainfall systems in China. *Adv. Atmos. Sci.*, **32**(2), 192–205, doi: 10.1007/s00376-014-0005-x.

## 1. Introduction

China is located in the Asian Summer Monsoon (ASM) region, featuring great fluctuations in precipitation. In South China, the rainy season comes following onset of the monsoon. During this period, torrential rainfall and flooding disasters often occur, bringing grave losses to the national economy, catastrophic damage to property, and frequent injury and death to the human population. The earliest written record of calamitous torrential rainfall in China dates back 2000 years ago, and rainfall events are closely linked with the record of human struggles against flooding. Due to tropical depressions or hurricanes, many regions in the world, such as India and the eastern Americas, also suffer from torrential rainfall. Therefore, the disasters induced by torrential rainfall

are a global problem.

Tao et al. (1980) systematically probed for the synoptic patterns favoring torrential rainfall occurrence. Based on these former studies, Chinese meteorologists pursued rainfall studies in detail and many important achievements were obtained. There are four main categories of torrential rainfall in China: typhoon rainfall; frontal rainfall; westerly trough rainfall; and low vortex rainfall. As is well-known, typhoons are one of the main disaster-causing weather systems in the eastern region of China; gales, torrential rain and storm tides caused by typhoons bring severe harm to the national economy and people’s lives and properties. Typhoons are the strongest rainstorm systems. For instance, Typhoon Carla (1962) brought extraordinary rainfall to Xinliao, Taiwan, with precipitation of up to 1248 mm in 24 hours. The global precipitation records for 24-hour and 3-day rainfall are 1870 mm and 3240 mm, respectively, both at Tin Rouse, Reunion Island in the Indian Ocean, also caused by a typhoon.

\* Corresponding author: GAO Shouting  
Email: gst@mail.iap.ac.cn

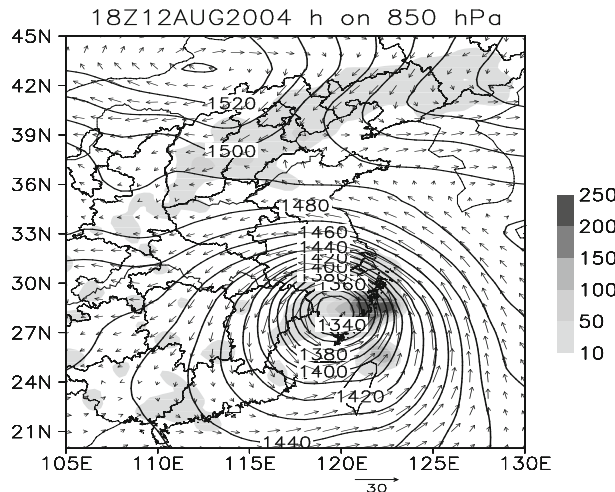


**Fig. 1.** Typhoon rainfall: geopotential height field at 850 hPa (contours; units: 10 flow), wind (vectors), and 6-h accumulative precipitation (shaded) at 1200 UTC 12 August 2004.

Typhoon rainfall includes inner core region precipitation, spiral rainbands, and the peripheral rainfall caused by the storm's interaction with adjacent circulation and topography (Fig. 1).

Frontal rainfall is extensive in China and often triggers flooding disasters. For instance, the rain before the summer monsoon is frontal rain in South China. The mei-yu front rainfall usually occurs during the period of June to July over the Yangtze River Basin, and can extend to Japan and Korea (Fig. 2). The mei-yu front is an important weather system that often generates torrential rainfall. North China, meanwhile, is affected by a westerly trough, which is an important part of the synoptic pattern. Torrential rainfall generated in front of

this westerly trough has triggered disastrous flooding in the region (Fig. 3). Furthermore, low-level vortices often spawn torrential rainfall in Northeast China and Southwest China, frequently resulting in local flooding. Vortex-induced rainfall has been much studied by Chinese meteorologists (Fig. 4).

There are many open questions in the field of torrential rainfall, and much additional work is needed to answer them. To avoid excessive length, this review will focus only on the dynamics of torrential rain. The first part of the main body of the paper (section 2) concentrates on studies incorporating moisture more realistically into atmospheric models and theory. Section 3 reviews progress on vorticity dynamics associated with rainfall. Frontal dynamics is discussed in section 4, and studies on wave dynamics are reviewed in section 5. The last part is a summary.

## 2. Study of moist atmosphere related with torrential rainfall

Rain is always closely associated with water vapor convergence, transportation and phase changes. Therefore, the water vapor budget and moisture physics are of great importance to the study of torrential rainfall.

### 2.1. Generalized moist potential temperature and generalized moist potential vorticity

The atmosphere is not saturated everywhere and the relative humidity is a little different from 100% in rain clouds due to turbulence and entrainment of dry air. In fact, water vapor is more liable to condense as the relative humidity gets higher, i.e. condensation grows with the relative humidity increase.

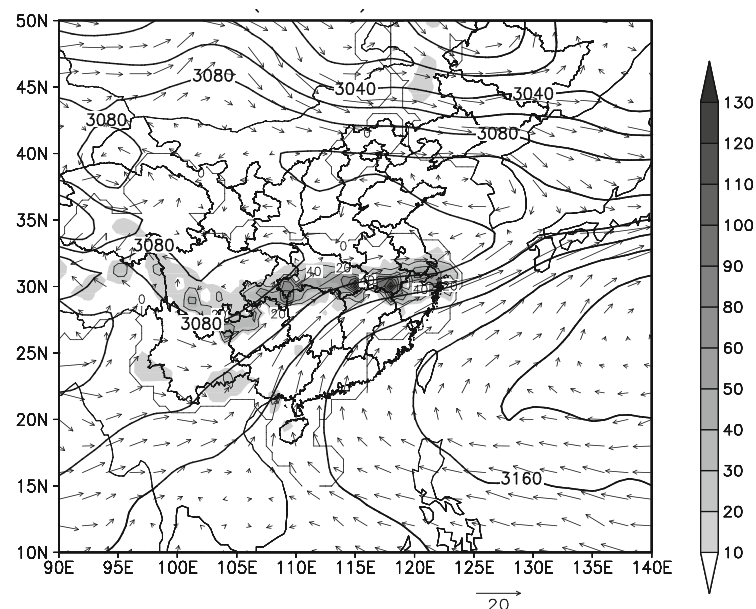


**Fig. 2.** Mei-yu rainfall: geopotential height field at 700 hPa (contours; units: 20 gpm), wind (vectors), and 6-h accumulative precipitation (shaded, units: mm) at 1800 UTC 26 June 1999.

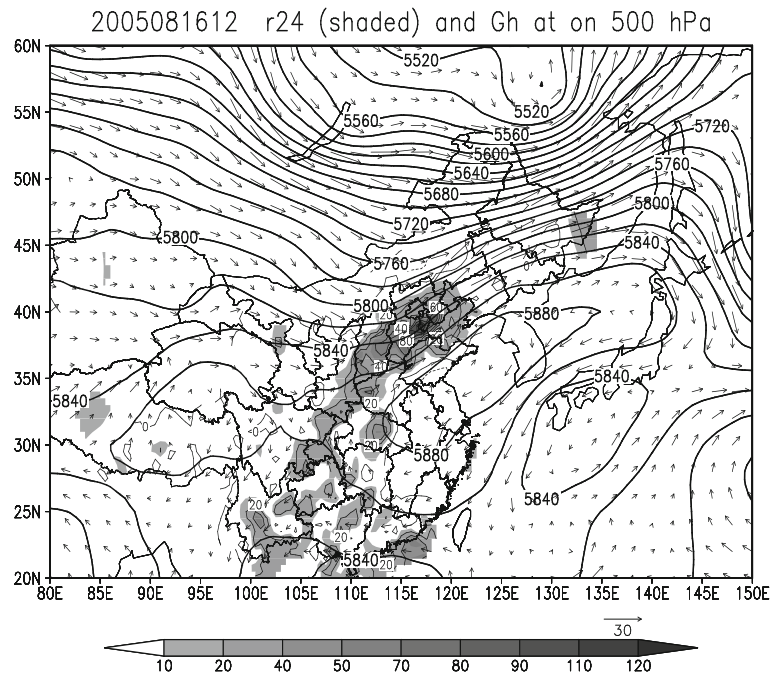


**Fig. 3.** Westerly trough rainfall, geopotential height field at 500 hPa (contours; units: 20 gpm), wind (vectors), and 24-h accumulative precipitation (shaded, units: mm) at 0400 UTC 16 August 2005.

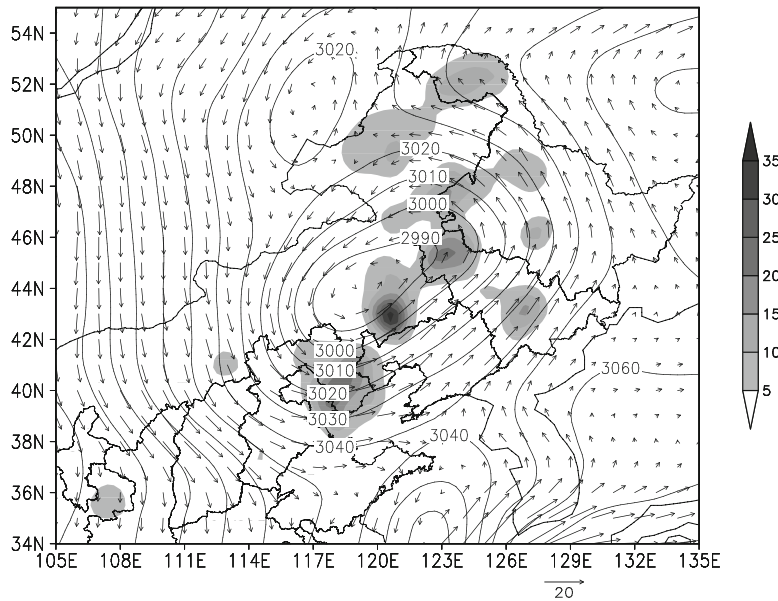


**Fig. 4.** Northeast Cold Vortex rainfall, geopotential height field at 700 hPa (contours; units: 10 gpm), wind (vectors), and 6-h accumulative precipitation (shaded) at 2200 UTC 9 July 2007.

Potential temperature  $\theta$  is a crucial physical variable which reflects the thermodynamic state of the atmosphere, and is conserved in frictionless, adiabatic flow following the motion. It is used to compare thermal differences between air parcels under different pressures to analyze the stability of the atmosphere (Schultz and Schumacher, 1999; Shou et al., 2003). Torrential rainfall releases much latent heat, so po-

tential temperature is no longer conserved. Therefore, equivalent potential temperature  $\theta_e$  was introduced because it is conserved even during heavy rainfall.

The rationale for defining  $\theta_e$  is as follows. An air parcel is saturated when it ascends to its condensation level. If there is uniform saturation in the air parcel, there should be rapid condensation and precipitation. Observationally, how-

ever, this is often not the case, which suggests the saturation of parcels in reality is not uniform. Gao et al. (2004a) therefore incorporated non-uniform saturation into the definition of a new potential temperature called generalized moist potential temperature (GMPT)  $\theta^*$  by adding a dimensionless condensation weight function:

$$\theta^* = \theta \exp \left[ \frac{Lq_s}{c_p T} \left( \frac{q}{q_s} \right)^k \right], \quad (1)$$

where  $T$  and  $\theta$  are the temperature and potential temperature, respectively;  $c_p$  is the specific heat of dry air;  $L$  is the latent heat of vaporization; and  $q$  and  $q_s$  are the unsaturated and saturated specific humidity, respectively.  $(q/q_s)^k$  is named as the condensation probability function,  $k$  is a power index, which is generally 9.

Gao et al. (2004a) proved that  $\theta^*$  is conserved following the motion in moist adiabatic flow. Furthermore, GMPT can be used in various conditions such as in dry, saturated and non-uniformly saturated air because it is conserved both in dry and moist adiabatic processes. It is a useful tool to diagnose atmospheric stability and to trace air parcel motion, and has a broader prospect for applications, such as to torrential rainfall, fog and heat waves. The comparison in diagnosing rainfall event between  $\theta^*$  and  $\theta_e$  is shown in Fig. 5. The large

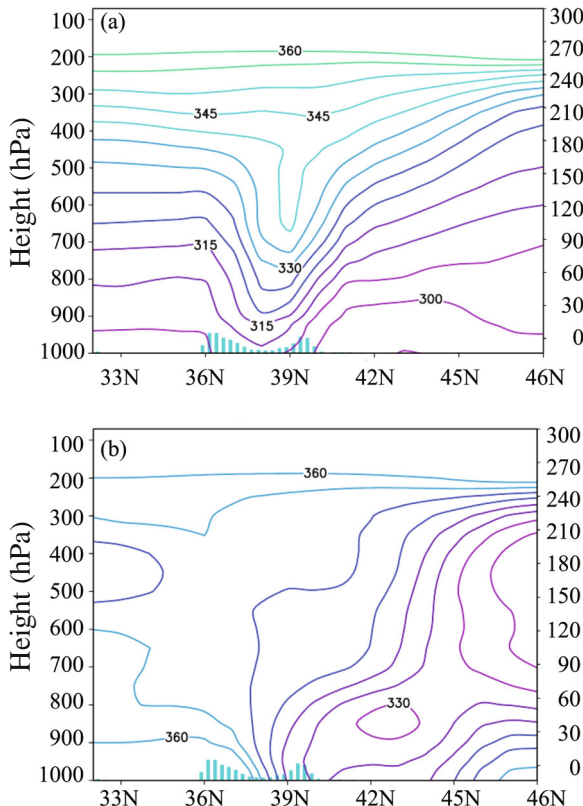


**Fig. 5.** Vertical–meridional cross sections of (a)  $\theta^*$  (contours; units: K) and (b)  $\theta_e$  (contours; units: K) of a rainfall event at 1200 UTC 12 August 2004. Bars represent precipitation (units: mm).

gradient region of  $\theta^*$  corresponds better to the rainfall area than that of  $\theta_e$ .

Potential vorticity (PV) is an important dynamical variable. Ertel derived PV for baroclinic flow in 1942:

$$PV = \frac{1}{\rho} \zeta_a \cdot \nabla \theta, \quad (2)$$

where  $\rho$  is the density, and  $\zeta_a$  is the 3D absolute vorticity vector. PV is conserved for adiabatic and frictionless motion in dry air. In torrential rain, however, particles initially at low levels are lifted into upper levels by strong updrafts, which creates upper-level PV anomalies. Such anomalies can serve as indicators for convection and rain. Another extremely important concept is the potential vorticity inversion (PVI) principle, which is the idea that one can not only use PV as a Lagrangian tracer but also to deduce balanced flow entirely from this single field (Kleinschmidt, 1957). Also, PV is not conserved when latent heat is released. Bennetts and Hoskins (1979) therefore generalized PV into moist potential vorticity (MPV), defined as

$$MPV = \frac{1}{\rho} \zeta_a \cdot \nabla \theta_e, \quad (3)$$

by replacing  $\theta$  with the equivalent potential temperature  $\theta_e$ . MPV has been extensively used in studies of conditional symmetric instability (Emanuel, 1983).

However, moist air in torrential rainfall systems is non-uniformly saturated; neither PV nor MPV is quite suitable for its description. Therefore, a generalized moist potential vorticity (GMPV) based on MPV was invented by Gao et al. (2004a). The definition is

$$GMPV = \frac{1}{\rho} \zeta_a \cdot \nabla \theta^*, \quad (4)$$

where  $\theta^*$  is the generalized potential temperature. Although GMPV is neither conserved nor invertible, it still is highly useful for torrential rain since it is a strong signal in diagnosing and analyzing rainfall. Here, a heavy rainfall in North China from 0000 UTC 27 June to 0600 UTC 27 June 2001 is illustrated (Fig. 6a). Figures 6b and c show that rainfall areas coincide with the distribution of GMPV at 850 hPa, while the distribution of MPV fails to describe the rainfall areas effectively.

## 2.2. Moist ageostrophic $Q$ vector

Vertical motion, one of the most important factors for cloud and precipitation, is closely associated with the development of torrential rain. Since the late 1970s, the  $\omega$  equation has become a vital approach to calculate vertical motion (Dunn, 1991) because the accuracy of vertical velocity affects the rainfall forecast directly. Vertical motion estimation draws much attention all around the world. Hoskins and Bretherton (1972) introduced a quasi-geostrophic  $Q$  vector, a unique forcing term in the  $\omega$  equation, and calculated this vector using single-level observational data. Once the  $Q$  vector is obtained, the vertical velocity can be diagnosed, as is now routine in operational service.

The  $\mathbf{Q}$  vector has been praised as a marvelous tool for diagnosing the vertical motion (Dunn, 1991). Consequently, many modifications and improvements of the  $\mathbf{Q}$  vector have been made, including the generalized  $\mathbf{Q}$  vector (Davies-Jones, 1991), the  $\mathbf{C}$  vector (Xu, 1992), the ageostrophic  $\mathbf{Q}$  vector (Zhang, 1999), and the moist ageostrophic  $\mathbf{Q}$  vector (Yao et al., 2004).  $\mathbf{Q}$  vectors have successfully been applied to torrential rainfall, heavy snow, etc.

All the expressions associated with the above-mentioned  $\mathbf{Q}$  vectors were derived under the condition that the atmosphere is either absolutely dry or uniformly saturated. Following Gao et al. (2004a), Yang et al. (2007) proposed a moist ageostrophic  $\mathbf{Q}$  vector for non-uniformly saturated flow, which is denoted by  $\mathbf{Q}_{\text{um}}$ . The ageostrophic diabatic  $\omega$

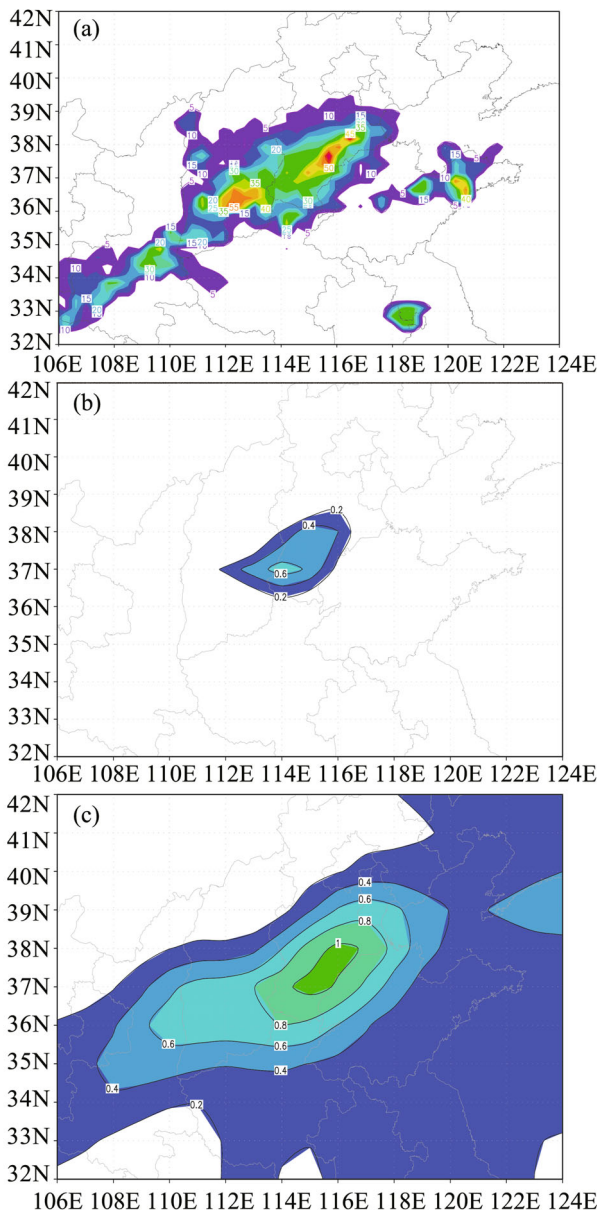


**Fig. 6.** (a) Precipitation in North China from 0000 UTC 27 June to 0600 UTC 27 June 2001. units: mm; (b) MPV at 850 hPa. units: PVU; (c) GMPV at 850 hPa. units: PVU.

equation including the diabatic effect can be written as

$$f \frac{\partial^2 \omega}{\partial p^2} + \nabla^2(\sigma \omega) = -2\nabla \cdot \mathbf{Q}_{\text{um}}, \quad (5)$$

where  $f$  is the Coriolis parameter,  $\omega$  is the vertical component of wind in the pressure coordinate, and  $\sigma$  is a parameter of static stability. This shows that  $\nabla \cdot \mathbf{Q}_{\text{um}}$  is the single forcing term in the ageostrophic diabatic  $\omega$  equation. When the  $\omega$  field displays sinusoidal features, one can argue that  $\omega \propto \nabla \cdot \mathbf{Q}_{\text{um}}$ . Thus, if  $\nabla \cdot \mathbf{Q}_{\text{um}} < 0$  ( $\nabla \cdot \mathbf{Q}_{\text{um}} > 0$ ), then  $\omega < 0$  ( $\omega > 0$ ), corresponds to upward (downward) motion. The above relation indicates that the convergence of  $\mathbf{Q}_{\text{um}}$  ( $\nabla \cdot \mathbf{Q}_{\text{um}} < 0$ ) gives rise to a secondary circulation with ascending motion, which is propitious for torrential rainfall.

If only the latent heat is considered, the two components of  $\mathbf{Q}_{\text{um}}$  are

$$\mathbf{Q}_{\text{um},x} = \frac{1}{2} \left( f \left( \frac{\partial v}{\partial p} \frac{\partial u}{\partial x} - \frac{\partial u}{\partial p} \frac{\partial v}{\partial x} \right) - h \frac{\partial \mathbf{V}}{\partial x} \cdot \nabla \theta - \frac{\partial}{\partial x} \cdot \left\{ \frac{LR}{c_p P} \frac{d}{dt} \left[ q_s \left( \frac{q}{q_s} \right)^k \right] \right\} \right) \quad (6)$$

and

$$\mathbf{Q}_{\text{um},y} = \frac{1}{2} \left( f \left( \frac{\partial v}{\partial p} \frac{\partial u}{\partial y} - \frac{\partial u}{\partial p} \frac{\partial v}{\partial y} \right) - h \frac{\partial \mathbf{V}}{\partial y} \cdot \nabla \theta - \frac{\partial}{\partial y} \cdot \left\{ \frac{LR}{c_p P} \frac{d}{dt} \left[ q_s \left( \frac{q}{q_s} \right)^k \right] \right\} \right), \quad (7)$$

where  $u$  and  $v$  are the zonal and meridional wind in the pressure coordinate, respectively, and  $\mathbf{V}$  is the wind vector,  $R$  is the gas constant. The above are the expressions of  $\mathbf{Q}_{\text{um}}$  in a non-uniformly saturated, frictionless, moist adiabatic flow.

$\mathbf{Q}_{\text{um}}$  is generalized only in almost saturated regions by the effect of the condensation probability function  $(q/q_s)^k$ . Through comparing the original  $\mathbf{Q}$  vector with  $\mathbf{Q}_{\text{um}}$ , it is found that the  $\mathbf{Q}_{\text{um}}$  is a better vector in diagnosing and predicting rainfall.

Yang et al. (2007) used  $\mathbf{Q}_{\text{um}}$  to diagnose heavy rainfall over the middle and lower reaches of the Yangtze River in China from 0600 UTC 4 July to 1200 UTC 5 July 2003. The case analyses demonstrate that  $\nabla \cdot \mathbf{Q}_{\text{um}}$  is a good predictor for the 6-h precipitation forecast. Since  $\nabla \cdot \mathbf{Q}_{\text{um}}$  is a forcing term in the ageostrophic diabatic  $\omega$  equation, convergence of  $\mathbf{Q}_{\text{um}}$  strengthens the ascending motion and secondary circulation, which are closely related to torrential rainfall.

### 2.3. Mass forcing effect of torrential rain

Torrential rain with amounts over 500 mm sometimes occurs in China. For example, Typhoon Nina (7503) brought about extraordinary torrential rainfall within Henan Province with accumulated precipitation of up to 1060 mm in 24 hours in August 1975. Taiwan also has a high frequency of torrential rain. On 8 August 2009, rainfall episodes at 14 stations were over 1000 mm. In particular, 1403 mm of rainfall at Weiliaoshan on that day broke the all-time daily cumulative precipitation record for the island. Huge amounts of liquid

water drops falling down to the ground must lead to mass deficiency in the moist air. Therefore, mass conservation of water vapor in the moist air is destroyed. Gu and Qian (1991) made comparison experiments using the PSU–NCAR (Pennsylvania State University–National Center for Atmospheric Research) mesoscale model and discussed the function of the source (or sink) term in the moist air continuity equation and other relevant equations. When heavy rainfall occurs, the source/sink terms in the moist air continuity equation, surface pressure tendency equation and vertical velocity equation will enhance the positive feedback caused by moisture condensation. Gray et al. (1998) utilized a mass forcing model to investigate how the PV anomalies respond to changes caused by convection. However, the model only considers the vertical mass transfer, and a mass convergence (divergence) zone occurred due to the convective activity transported upward (downward). Although all of the studies mentioned above include a source/sink term, the total mass is still conserved. Using the PSU–NCAR mesoscale model, Qiu et al. (1993) found that the effect of mass sinks (or sources) could have a significant impact on numerical simulations of heavy precipitation. When mass sinks are ignored, precipitation is reduced in the model. Gao et al. (2002) studied the MPV anomalies with both heat and mass forcings following Qiu et al. (1993) through the mass loss due to the intensive precipitation in torrential rain. For large-scale systems, external forcing is mainly the heat forcing and frictional dissipation. In contrast, for mesoscale convective systems, the MPV anomaly is mainly from mass forcing. Since there is intensive rainfall in the convective system, the change of the internal mass field is dominated not only by the convergence or divergence in the background field, but also by the remarkable mass decrease caused by torrential rainfall.

The continuity equations are (Gao et al., 2004a)

$$\frac{\partial \rho_d}{\partial t} + \nabla \cdot (\rho_d \mathbf{V}) = 0, \quad (8)$$

$$\frac{\partial \rho_m}{\partial t} + \nabla \cdot (\rho_m \mathbf{V}) = -Q_m, \quad (9)$$

$$\frac{\partial \rho_r}{\partial t} + \nabla \cdot [\rho_r (\mathbf{V} + \mathbf{V}_t)] = Q_m, \quad (10)$$

where  $\rho_d$ ,  $\rho_m$  and  $\rho_r$  are the density of dry air, water vapor and condensate (precipitation), respectively.  $Q_m$  is the condensation rate that forms airborne cloud water and rain water, and  $\mathbf{V}_t$  is the terminal velocity of the raindrops. The density of the moist air is  $\rho_2 = \rho_d + \rho_m$  and the total density is  $\rho_3 = \rho_d + \rho_m + \rho_r$ . Add the three equations together and the following equation can be derived:

$$\frac{\partial \rho_3}{\partial t} + \nabla \cdot (\rho_3 \mathbf{V}) = -\nabla \cdot (\rho_r \mathbf{V}_t) = S, \quad (11)$$

where  $S = -\nabla \cdot (\rho_r \mathbf{V}_t)$  represents the contribution of the mass forcing induced by precipitation.

Gao et al. (2002) deduced the MPV equation with heat and mass forcings to show that intensive rainfall can generate MPV anomalies under heat and mass forcings. The MPV

equation with these two forcings on the frictionless and adiabatic saturation condition is

$$\frac{\partial}{\partial t} \left( \frac{\boldsymbol{\omega}_a \cdot \nabla \theta_e}{\rho} \right) = -\mathbf{V} \cdot \nabla \left( \frac{\boldsymbol{\omega}_a \cdot \nabla \theta_e}{\rho} \right) - \frac{S}{\rho} \left( \frac{\boldsymbol{\omega}_a \cdot \nabla \theta_e}{\rho} \right), \quad (12)$$

where  $\boldsymbol{\omega}_a$  is the absolute vorticity vector,  $\theta_e$  is equivalent potential temperature, and  $\rho$  is density. This equation is suitable to study torrential rain systems and other severe weather systems, while the traditional PV or MPV theory considers only the heat forcing or only the friction forcing.

### 3. Progress in vorticity dynamics

#### 3.1. Slantwise vorticity development

In 1942, Ertel put forth the concept of PV, which is a conserved quantity in a frictionless and adiabatic dry atmosphere. Hoskins et al. (1985) summarized the applications of Ertel PV in the diagnosis of atmospheric motion, and introduced isentropic potential vorticity (IPV). In general, IPV is indicative of some aspects of the movement and development of weather systems in middle and high latitudes. However, in the lower troposphere, especially in low latitudes, IPV becomes very weak. Besides, IPV does not include the effects of moisture. In short, the application of IPV analysis has limitations in the lower troposphere, low latitude regions and in precipitation cases. Considering the moisture effects, the conservation of MPV was obtained. Based on the conservation characteristics of PV and MPV, when the isentropic surfaces appear to be declining under which condition the application of IPV is restricted, slantwise vorticity development (SVD) theory was created to show a mechanism of lower tropospheric vertical vorticity development that can induce the torrential rain.

A front is a slantwise interface. Thus, there is a sharp temperature contrast near the interface. The front can be described by a slanting isentropic surface near which vorticity is apt to develop. In fact, since many kinds of weather systems develop slanting (moist) isentropic surfaces, it is necessary to investigate the evolution of these systems in the context of slantwise isentropic surfaces (Cui et al., 2003). On the basis of the conservation of Ertel PV and MPV, Wu and Liu (1997) used a “parcel dynamics” approach to investigate vertical vorticity development near the slanting isentropic surface, which they interpreted as SVD. A new form of the tendency equation of vertical vorticity was then deduced.

In adiabatic, frictionless atmosphere, Ertel PV is conserved:

$$P_E = \alpha \zeta_z \frac{\partial \theta}{\partial z} + \alpha \zeta_s \frac{\partial \theta}{\partial s} = \text{constant}, \quad (13)$$

where  $P_E$  is Ertel PV,  $z$  is the usual height coordinate,  $\alpha$  is specific volume,  $\partial \theta / \partial s$  is the horizontal gradient of potential temperature  $\theta$ ,  $\zeta_z$  is the vertical component of absolute vorticity  $\boldsymbol{\zeta}_a$ , and  $\zeta_s$  is the projection on  $s$  of  $\boldsymbol{\zeta}_a$ , which is determined by the vertical shear of the wind.

It can be shown that

$$P_E = \alpha \zeta_z \frac{\partial \theta}{\partial z} + \alpha \zeta_s \frac{\partial \theta}{\partial s} = \alpha \zeta_\theta \frac{\partial \theta}{\partial n} = \text{constant}, \quad (14)$$

where  $\zeta_\theta$  is the projection of  $\zeta_a$  on  $\nabla \theta$ . If the absolute vorticity per unit mass is denoted by  $\xi_a = \alpha \zeta_a$ , and  $\xi_n = \alpha \zeta_\theta$ , then the above relation can be rewritten as

$$P_E = \xi_z \theta_z + \xi_s \theta_s = \xi_n \theta_n = \text{constant}. \quad (15)$$

Furthermore,

$$\xi_z = (\xi_n \theta_n - \xi_s \theta_s) / \theta_z, \quad (\theta_z \neq 0). \quad (16)$$

This means that the change of vertical vorticity can result from the changes in static stability  $\theta_z$ , vertical wind shear  $\zeta_s$ , or baroclinity  $\theta_s$ .

The schematic chart of SVD [Fig. 2 in Wu and Liu (1997)'s study] shows how the slope of the isentropic surface affects the change of vertical vorticity. The parallel isentropes are assumed to be horizontal to the right of the  $z$ -coordinate, but bent as circles to its left. The slope angle  $\beta$  is positive when one side deviates from  $z$  to  $s$ . The gradient of isentropes  $\theta_n$  is constant. When  $C_D = \xi_s \theta_s / \theta_z < 0$  is satisfied,  $\xi_z = (\xi_n / \cos \beta + |\xi_s \tan \beta|)(|\beta| \neq \pi/2)$  can be obtained. It means that when an air parcel is sliding down the slope of a  $\theta$  surface, its vertical vorticity will increase as long as the above condition is satisfied.  $\xi_z$  can be extremely large when the slope of the  $\theta$  surface is sharply steep, and the increase of vertical vorticity is due to the down-sliding of the air parcel along a slantwise isentropic surface, which can be referred to as down-sliding SVD.

A new form of the tendency equation for the vertical vorticity component  $\xi_z$  is then:

$$\begin{aligned} \frac{D\xi_z}{Dt} + \beta v + (f + \xi_z) \nabla \cdot \mathbf{V} = -\frac{1}{\alpha \theta_z^2} \left[ (P_E - \xi_s \theta_s) \frac{D\theta_z}{Dt} + \right. \\ \left. \theta_z \xi_s \frac{D\theta_s}{Dt} + \theta_z \theta_s \frac{D\xi_s}{Dt} \right], \\ (\theta_z \neq 0). \end{aligned} \quad (17)$$

The equation indicates that the changes of static stability, baroclinity and vertical wind shear can affect the development of vertical vorticity. A numerical experiment was performed for a southwest vortex rainfall event from 11 to 15 July 1981 in Sichuan Province. Based on the adiabatic model of Bleck (1984), with  $\theta$  as the vertical coordinate, the formation of this vortex was simulated. Vertical vorticity developed along the eastern edge of the Tibetan Plateau and a new-born cyclonic vortex appeared in the region where the wind vectors slid down the steeply tilted  $\theta$  surface. This case study shows that vortex development can be well explained with SVD theory.

The theory of down-sliding SVD was then extended from the dry atmosphere to a moist atmosphere with the assumptions that the atmosphere is saturated and the speed of a

down-sliding parcel at a surface is slow enough that the properties of the parcel are well mixed with those of the environment. For an adiabatic, frictionless moistly saturated atmosphere, the MPV is conserved (Bennetts and Hoskins, 1979, Wu and Blumen, 1995):

$$\frac{DP_m}{Dt} = 0, \quad (18)$$

where  $P_m$  is moist potential vorticity. Similarly, in Fig. 6 of Wu and Liu (1997), the parallel moist isentropes  $\theta_e$  are assumed to be horizontal to the left of the  $z$ -coordinate, but are bent as circles to its right. The gradient of  $\theta_e$  is constant. In Fig. 6 of Wu and Liu (1997), down-sliding corresponds to the increase of the down-slope angle  $\beta$  (defined as before), whereas in Fig. 2 of Wu and Liu (1997) down-sliding corresponds to the decrease of  $\beta$ . A formula similar to Eq. (16) is obtained:

$$\xi_z = (\xi_n \theta_{e,n} - \xi_s \theta_{e,s}) / \theta_{e,z}, \quad (\theta_{e,z} \neq 0). \quad (19)$$

If the condition  $\frac{dC_M}{dt} < 0$  ( $C_M = \theta_{e,s} \xi_s / \theta_{e,z}$ ) is assumed, then a new form of the vertical vorticity tendency equation for a saturated atmosphere can be obtained as

$$\begin{aligned} \frac{D\xi_z}{Dt} + \beta v + (f + \xi_z) \nabla \cdot \mathbf{V} = -\frac{1}{\alpha \theta_{e,z}^2} \left[ (P_E - \xi_s \theta_{e,s}) \frac{D\theta_{e,z}}{Dt} + \right. \\ \left. \theta_{e,z} \xi_s \frac{D\theta_{e,s}}{Dt} + \theta_{e,z} \theta_{e,s} \frac{D\xi_s}{Dt} \right], \\ (\theta_{e,z} \neq 0). \end{aligned} \quad (20)$$

The SVD condition for  $\zeta_z$  or  $\xi_z$  in saturated atmosphere becomes

$$\frac{dC_M}{dt} < P_m \left[ \frac{1}{\theta_{e,z}(t + \Delta t)} - \frac{1}{\theta_{e,z}(t)} \right], \quad \theta_{e,z} \neq 0 \quad (21)$$

or

$$C_M(\beta + \Delta\beta) - C_M(\beta) < P_m \left[ \frac{1}{\theta_{e,z}(\beta + \Delta\beta)} - \frac{1}{\theta_{e,z}(\beta)} \right], \\ \theta_{e,z} \neq 0. \quad (22)$$

SVD will occur so long as the condition (21) or (22) is satisfied, and it can be seen that the condition  $dC_M/dt < 0$  is a sufficient condition for SVD.

### 3.2. Convective vorticity vector

Gao et al. (2004a) found that PV has some limitations when it is applied to deep tropical convection in the equatorial area. In a 2D dynamical frame, the absolute vorticity can be expressed as

$$\boldsymbol{\omega}_a = \left( \frac{\partial u}{\partial z} - \frac{\partial w}{\partial x} + 2\Omega \cos \varphi \right) \mathbf{j} + 2\Omega \sin \varphi \mathbf{k}, \quad (23)$$

where  $\Omega$  is the earth rotating angle speed, and the gradient of equivalent potential temperature is  $\nabla \theta_e = \partial \theta_e / \partial x \mathbf{i} + \partial \theta_e / \partial z \mathbf{k}$ . Thus, the 2D PV is

$$\boldsymbol{\omega}_a \cdot \nabla \theta_e / \rho = \frac{2\Omega \sin \varphi}{\rho} \frac{\partial \theta_e}{\partial z}. \quad (24)$$

In the tropics, the moist isentropic surfaces are nearly vertical in deep convective systems, and their vertical gradients are very small, with  $\partial\theta_e/\partial z$  approaching zero. Furthermore, the Coriolis force near the equator is small (because  $\sin\varphi \approx 0$  at the equator, and thus  $2\Omega\sin\varphi \approx 0$ ). Because of all the factors above, the value of the 2D PV is very small or even zero. Likewise, the analysis above can be applied to deep convective systems with torrential rainfall. Moist isentropic surfaces tend to be vertical and  $\nabla\theta_e$  shifts to be almost zonal due to the intense convection and moist saturation. The dot product of absolute vorticity and equivalent potential temperature is a weak signal.

In the 3D dynamical frame (Gao et al., 2007), the tropical atmosphere is nearly barotropic and the vertical shear of the zonal wind is weak, i.e. the value of  $\partial u/\partial z$  and  $\partial v/\partial z$  is small. The moist isentropic surfaces are mostly upright in deep convective systems ( $\partial\theta_e/\partial z \approx 0$ ), and the 3D PV can be accurately approximated as

$$\boldsymbol{\omega}_a \cdot \nabla\theta_e/\rho \approx \frac{\partial w}{\partial y} \frac{\partial\theta_e}{\partial x} - \frac{\partial w}{\partial x} \frac{\partial\theta_e}{\partial y}, \quad (25)$$

and also alternatively be written as  $\boldsymbol{\omega}_a \cdot \nabla\theta_e/\rho \approx |\nabla_h\theta_e| |\nabla_h w| \sin\alpha$ . When the angle  $\alpha$  of  $\nabla_h\theta_e$  and  $\nabla_h w$  in the horizontal plane is small, the value of the 3D PV is also very small. Therefore, both the 2D and 3D PVs are weak signals for tropical deep convection systems and might be confused with the noise or calculated errors. Hence, PV is severely handicapped for diagnosing tropical convection.

To solve this problem, Gao et al. (2004b) introduced a new vector, the convective vorticity vector (CVV), defined as  $\text{CVV} = \boldsymbol{\omega}_a \times \nabla\theta_e/\rho$ , to study deep convection in the tropics. Different from the 2D PV, the vertical component  $[\mathbf{k} \cdot (\boldsymbol{\omega}_a \times \nabla\theta_e/\rho)] = (\partial w/\partial x)(\partial\theta_e/\partial x)$  of 2D CVV focuses on the characteristics of relatively large horizontal vorticity  $[-(\partial w/\partial x)\mathbf{j}]$  and equivalent potential temperature gradient  $[-(\partial\theta_e/\partial x)\mathbf{i}]$ , which are strong signals for 2D deep convection. Under the 3D dynamical frame, the vertical component of CVV can be expressed as

$$\mathbf{k} \cdot (\boldsymbol{\omega}_a \times \nabla\theta_e/\rho) = \frac{\partial w}{\partial y} \frac{\partial\theta_e}{\partial y} + \frac{\partial w}{\partial x} \frac{\partial\theta_e}{\partial x} = |\nabla_h\theta_e| |\nabla_h w| \cos\alpha. \quad (26)$$

It not only describes the combined dynamical and thermodynamical features of horizontal vorticity  $[(\partial w/\partial y)\mathbf{i} - (\partial w/\partial x)\mathbf{j}]$  and the horizontal gradient of equivalent potential temperature  $[(\partial\theta_e/\partial x)\mathbf{i} + (\partial\theta_e/\partial y)\mathbf{j}]$  in tropical deep convection, but also is a significant parameter when the angle  $\alpha$  between  $\nabla_h\theta_e$  and  $\nabla_h w$  is small, which implies that CVV is a strong signal of deep convection. From this tropical deep convection perspective, the CVV is markedly superior to the 3D PV. Both 2D and 3D CVVs can describe tropical deep convection. By testing the CVV using the 2D and 3D cloud-resolving NASA (National Aeronautics and Space Administration) models, it was demonstrated that the vertical component of CVV is a macroscopic quantity closely related to tropical deep convection.

#### 4. Progress in frontal dynamics

The concept of a weather front was first introduced by Bjerknes (1918). Later, Bjerknes and Solberg focused on the polar front and emphasized that it was a synoptic member in middle and high latitudes. Bergeron (1928) conceptualized frontogenesis as the confluence of two air masses with sharply different temperatures. Newton (1954), Reed (1955) and Reed and Danielsen (1958) analyzed the structure of upper fronts. Petterssen (1936) and Miller (1948) discussed the intensity of fronts through analyzing the Lagrangian change of the potential temperature gradient. Petterssen (1956) further pointed out that divergence and deformation are the major factors for frontogenesis.

In the 1960s, quasi-geostrophic frontogenesis was studied. However, it omitted the ageostrophic motion along fronts. Semi-geostrophic frontogenesis was used by Hoskins (1972) to describe the ageostrophic motion across the front. This was considered a major advance in frontogenesis theory. Both the quasi-geostrophic and semi-geostrophic frontogenesis theories, based on balanced frontogenesis models, describe the processes that are influenced by the large-scale forcing. Nevertheless, a few frontogenesis processes are not driven by the large-scale forcing, but by the initial unbalanced flow. Therefore, Blumen and Wu (1995) and Wu and Blumen (1995) described frontogenesis by invoking the geostrophic adjustment.

Based on the unbalance frontogenesis model, Fang and Wu (1998) discussed the transient adjustment and the conditions of geostrophic adjustment frontogenesis. Wang et al. (2000) conducted two experiments to reveal the roles of the initial temperature gradient, vapor distribution and orographic forcing on frontogenesis with ageostrophic-balanced initial fields using the 3D non-hydrostatic ARPS (Advanced Regional Prediction System) model. This study proposed the results as follow:

- (1) Without the large-scale forcing flow, frontogenesis could occur if the initial flow was sufficiently unbalanced;
- (2) With geostrophic adjustment, frontogenesis alternates with frontolysis, while vertical velocity and potential temperature gradient have visible oscillations;
- (3) Less than 50% of perturbation kinetic energy can be released to perturbation potential energy, and the released amount is associated with the initial perturbation scale.

Geostrophic adjustment frontogenesis theory describes rapid frontogenesis well. Blumen and Wu (1995) used a density-stratified model, following Ou (1984), to establish the relation between the frontogenetic initial and final states for zero PV flow.

Wu and Blumen (1982) and Blumen and Wu (1983) discussed Ekman boundary layer frontogenesis, which is the role of boundary friction on frontal evolution. Using a two-layer shallow water model including boundary layer friction, Tan and Wu (2000a,b) analyzed frontal circulation, showing that surface friction increases with low-level horizontal convergence, and therefore the vertical motion against the front is strengthened by the boundary-layer friction. Furthermore,

they analyzed boundary layer frontogenesis as the balance of four forces: pressure gradient force, Coriolis force, friction force and inertia force. They found that boundary-layer friction plays a dual role in frontogenesis; on the one hand, the frictional dissipation caused by the boundary layer is frontolytic, while on the other hand the friction in the boundary layer enhances the ageostrophic flow and is thus frontogenetic.

Wang and Wu (1999) investigated the interaction of orographic perturbations with a front to examine the impacts of orography on both frontogenesis and the low-level frontal structure. When the cold front moves toward a mountain, the warm air ahead of the cold front, slipping up the orography, enhances the convergence, which promotes ascending motion. Conversely, when the cold front is located on the lee side, the warm air gliding down along the mountain in front of the cold front weakens the convergence and the ascending flow. When the cold front crosses over the orography, ascent strengthens again and induces intermittent precipitation.

Wang and Wu (1999) discussed the positive feedback of diabatic heating upon the geostrophic adjustment. Strong diabatic heating results in the enhancement of the local thermal contrast and the destruction of the geostrophic equilibrium, which leads to geostrophic adjustment. Through this process, a positive feedback mechanism between the vertical circulation and diabatic heating can amplify the frontal discontinuity.

## 5. Wave dynamics

### 5.1. Mixed vortex–Rossby–inertia–gravity wave studies

Based on vortex–Rossby waves (VRWs) and inertial gravity waves (IGWs), which had been proposed to explain the propagation of spiral rainbands and the development of dynamical instability in tropical cyclones (TCs), Zhong et al. (2009, 2010) developed a theory for mixed vortex–Rossby–inertia–gravity waves (VRIGWs) coexisting with VRWs and IGWs, including both rotational and divergent flows in a shallow-water equations model. A cloud-resolving tropical cyclone simulation was used to justify the simplification of the radial structure equation for linearized perturbations and its subsequent transformation to an analytically soluble Bessel equation. A cubic frequency equation describing the three groups of allowable (radially discrete) waves was derived. It shows that low-frequency VRWs and high-frequency IGWs may coexist, but with distinct dispersion characteristics, in the eye and outer regions of TCs. In contrast, mixed VRIGWs with instability properties tend to occur in the eyewall. The mixed-wave instability, for which shorter waves grow faster than longer waves, appears to explain the generation of polygonal eyewalls and multiple vortices with intense rotation and divergence in tropical cyclones. High-frequency IGWs would propagate in the inner regions at half of typical VRIGW speeds and also display more radial “standing” structures. Moreover, all the propagating waves appear in the form of spiral bands but with different intensities as their ra-

dial widths shrink in time. This suggests that some spiral rainbands in TCs may result from the radial differential displacements of azimuthally propagating perturbations.

The barotropic stability of VRWs in 2D inviscid hurricane-like vortices is discussed in the context of rotational dynamics on an  $f$ -plane by Zhong et al. (2010). Two necessary conditions for vortex–barotropic instability are found:

(1) There must exist at least one point at which the radial gradient of basic-state vorticity vanishes;

(2) The radial propagation of the VRWs must be opposite to the vorticity gradient, which imposes a restriction on the growth of wave energy.

The maximum growth rate depends on the peak radial gradient of the basic-state vorticity and the tangential wavenumber (WN). Furthermore, these waves satisfy Howard’s semi-circle theorem, which provides bounds on the growth rates and wave phase speeds.

The typical structures of basic-state variables and different tangential WN perturbations in a TC were obtained from a high-resolution cloud-resolving simulation. The first necessary condition for instability can be easily met at the radius of maximum vorticity (RMV). The wave energy tends to decay (grow) inside (outside) the RMV due to the sign of the radial gradient of the basic-state absolute vorticity. This finding appears to help explain the development of strong vortices in the eyewall of TCs.

### 5.2. Wave–basic flow interaction in torrential rainfall

The gravity waves triggered by complex terrain and the associated wave breaking have been primary objectives of atmospheric dynamicists for a long time (Gao and Ran, 2003). Gravity wave studies improved the understanding of orographically influenced precipitation events and also related flooding episodes involving deep convection, frontal precipitation, and so on. In fact, although gravity waves are the primary phenomena in some catastrophic weather events, Rossby waves and inertial waves also account for some extreme weather events. Therefore, disturbances coupling all kinds of waves are responsible for extreme precipitation or convection. Among the various subfields of wave theory, wave–basic flow interaction is one of the most important.

Wave “activity” is an important concept for wave–basic flow interaction. Generally, the “wave activity” or “wave action density” was defined by Scinocca and Shepherd (1992) and Haynes (1988). It is a disturbance quantity that is quadratic or of higher order in disturbance amplitude in the small-amplitude and is subjected to a flux form of wave-activity law. In the past several decades, wave–basic flow interaction has been comprehensively investigated and a number of wave-activity laws have been constructed for multifarious intentions.

Large-scale circulation was the focus of most wave-mean interaction theory in the 1960s, 70s and 80s. Therefore, wave-activity theorems, restricted to quasi-geostrophic, hydrostatic flow but suitable for planetary waves and Rossby

waves, were thoroughly explored. On the other hand, wave-activity laws applicable to ageostrophic and nonhydrostatic mesoscale disturbances were largely ignored in spite of the immense practical significance of such disturbances, especially when accompanied by heavy rainfall. Because many early wave-activity theorems were restricted to a hydrostatic framework, they accurately reflected large-scale weather systems rather than mesoscale disturbances.

Scinocca and Shepherd (1992) derived a non-hydrostatic, finite amplitude wave-activity conservation law from a Hamiltonian system. However, their theories were confined to two spatial dimensions. Although the wave-activity laws

for 2D mesoscale systems worked well, they cannot be applied to a horizontally homogeneous background flow in a 3D framework because of the degeneracy created by the absence of a background PV gradient.

Ran and Gao (2007) derived a 3D, ageostrophic and non-hydrostatic local wave-activity law for pseudomomentum in Cartesian coordinates. In their derivation, the Haynes (1988) Momentum-Casimir method was extended and generalized. The advantage of this method is that a zonal or temporal average is not required to define the basic state, as with older theories. Therefore, it is propitious to investigate the 3D case. Shaw and Shepherd (2008) applied the Casimir technique

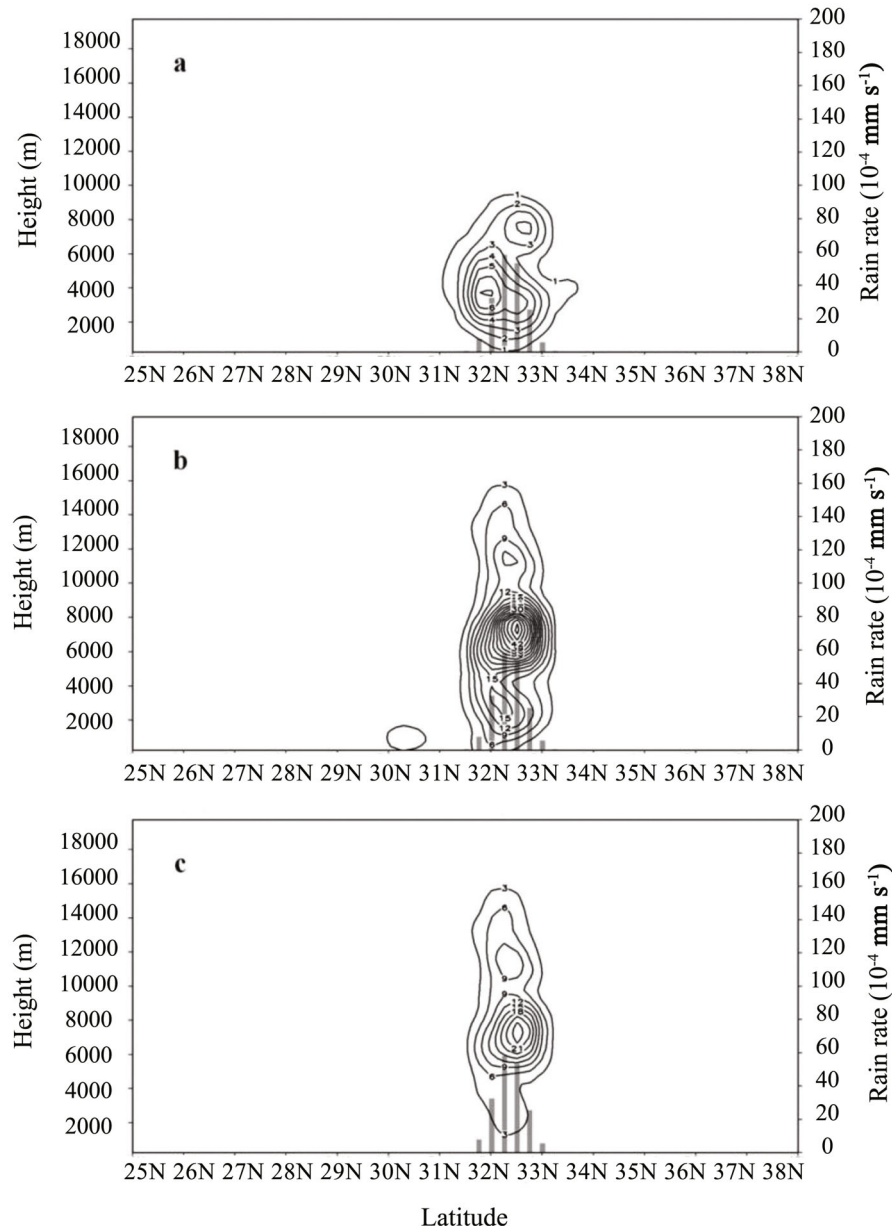


**Fig. 7.** Vertical–latitudinal cross sections of three specific wave-activity densities: (a)  $|A_{w_e1}|$  (units:  $10^{-14} \text{ m}^{-1} \text{ s}^{-1}$ ), (b)  $|A_{w_e2}|$  (units:  $10^{-11} \text{ K m}^{-1} \text{ s}^{-1}$ ), and (c)  $|A_{w_e3}|$  (units:  $10^{-11} \text{ K m}^{-1} \text{ s}^{-1}$ ) along  $118.5^\circ\text{E}$  at 0000 UTC 5 July 2003. The gray bars denote the rain rate (units:  $10^{-4} \text{ mm s}^{-1}$ ).

to 3D anelastic and Boussinesq equations with a horizontally homogeneous background flow, and derived 3D wave-activity conservation laws associated with energy and horizontal momentum. Their theory may be more applicable to mesoscale-gamma weather systems because they ignored the effects of Earth's rotation.

Moisture plays an important and sensitive role in heavy rainfall events, but it has often been excluded in studies of wave–basic flow interaction. This is not consistent with real-

ity when rainfall is heavy. Incorporating moisture, Gao and Ran (2009) developed 3D nonhydrostatic and ageostrophic general moist wave-activity laws, extending PV theorems, and then applied their theories to diagnose wave activity in a heavy rainfall storm over the Yangtze–Huaihe River valleys in China. Their case study showed that the three moist wave-activity densities shared a similar distribution pattern (Fig. 7) and temporal variation trends (Fig. 8) with the simulation's rate of precipitation. This indicated that there was

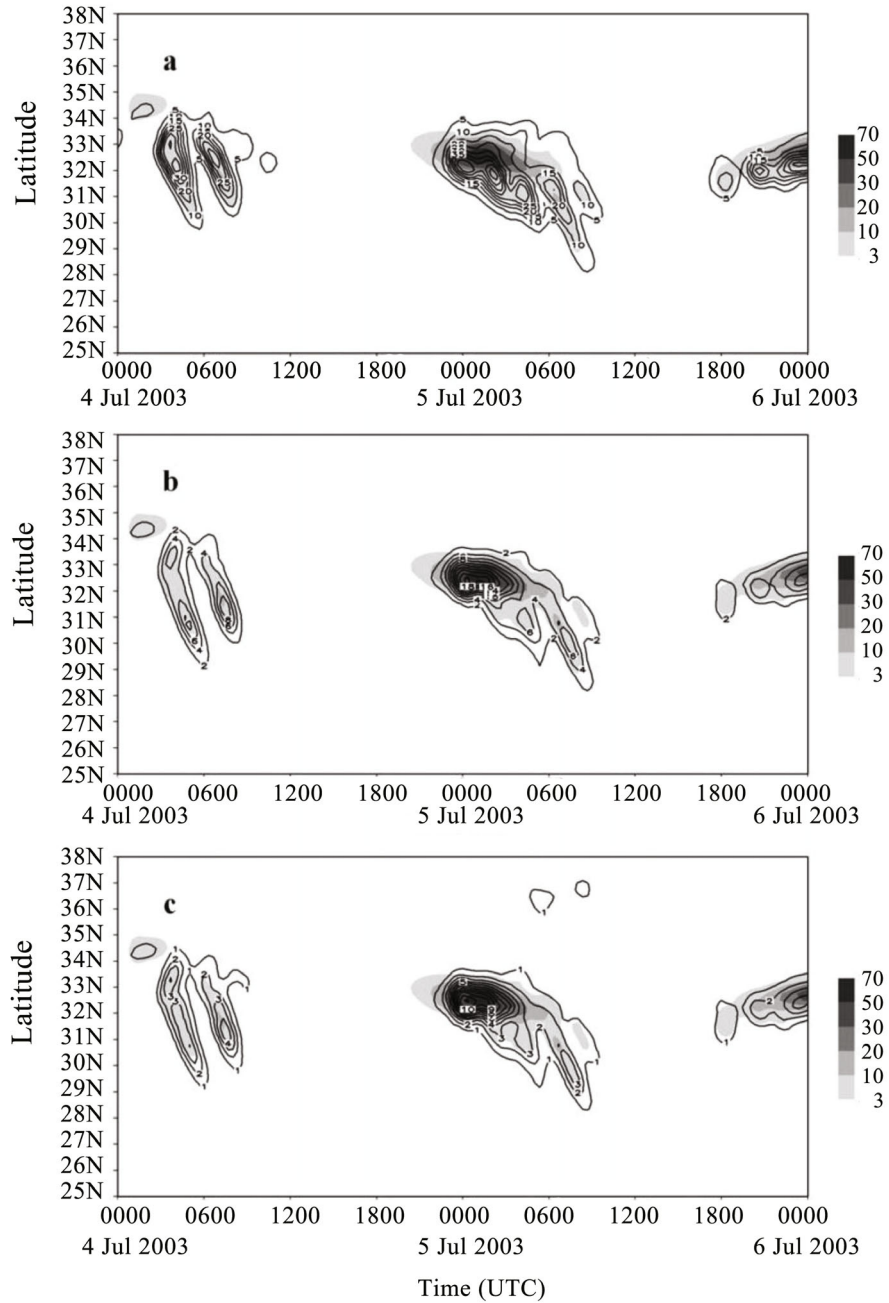


**Fig. 8.** Temporal–latitudinal cross sections of (a)  $\langle |A_{w_e1}| \rangle$  (units:  $10^{-11} \text{ s}^{-1}$ ), (b)  $\langle |A_{w_e2}| \rangle$  (units:  $10^{-7} \text{ K s}^{-1}$ ), and (c)  $\langle |A_{w_e3}| \rangle$  (units:  $10^{-7} \text{ K s}^{-1}$ ) zonally averaged over the longitudinal belt of  $118.5^\circ\text{--}121^\circ\text{E}$  from 0000 UTC 4 to 0000 UTC 6 July 2003. The gray shading denotes the rain rate (units:  $10^{-4} \text{ mm s}^{-1}$ ).

strong wave activity over the precipitation region. These investigations of wave activity extended the theory of wave–basic flow interaction from large-scale fields to mesoscale fields and thus enriched mesoscale atmospheric dynamics.

### 5.3. Balanced dynamics in typhoons

Lu et al. (2004) applied the concept of “gradient wind momentary approximation” to discuss the development of mesoscale disturbances in typhoons. The diagnostic equation for the streamfunction of the radial-and-vertical secondary circulation in cylindrical coordinate system was derived as

$$\begin{aligned} & \frac{1}{r} \frac{g}{\theta_0} \frac{\partial \theta}{\partial z} \frac{\partial^2 \psi}{\partial r^2} - \frac{2}{r} \left( \frac{2\tilde{v}}{r} + f \right) \frac{\partial \tilde{v}}{\partial z} \frac{\partial^2 \psi}{\partial r \partial z} + \\ & \frac{1}{r^2} \left( \frac{2\tilde{v}}{r} + f \right) \frac{\partial m}{\partial r} \frac{\partial^2 \psi}{\partial z^2} - \frac{1}{r^2} \frac{g}{\theta_0} \frac{\partial \theta}{\partial z} \frac{\partial \psi}{\partial r} + \\ & \left( \frac{1}{r^3} + \frac{3}{r^2} \right) \frac{g}{\theta_0} \frac{\partial \theta}{\partial r} \frac{\partial \psi}{\partial z} = 0, \end{aligned} \quad (27)$$

where  $\psi$  is the streamfunction and  $m$  is the isoline of momentum.  $\tilde{v}$  and  $\theta_0$  represents basic flow and initial potential temperature, respectively. Defining  $(g/\theta_0)(\partial\theta/\partial r) = S^2$ ,  $(g/\theta_0)(\partial\theta/\partial z) = N^2$ ,  $(2\tilde{v}/r + f)(1/r)(\partial m/\partial r) = F^2$ , the ellipticity condition for this partial differential equation is  $F^2N^2 - S^4 > 0$ , i.e.  $(\partial m/\partial r)_\theta(\partial\theta/\partial z) > 0$ . If, on the other hand,  $F^2N^2 - S^4 < 0$ , i.e.  $(\partial m/\partial r)_\theta(\partial\theta/\partial z) < 0$ , then the diagnostic equation is a partial differential equation of hyperbolic type. Obviously, satisfying both of the conditions  $[(\partial m/\partial r)_\theta > 0 \text{ and } \partial\theta/\partial z > 0]$  is sufficient but not necessary for the equation for the streamfunction to be of elliptic type. When  $(\partial m/\partial r)_\theta < 0, \partial\theta/\partial z > 0$  so the diagnostic relation is hyperbolic, and the flow also satisfies the conditions for inertial instability, a kind of symmetric instability.

The balanced model, which makes approximations that are sensible only when high-frequency waves such as gravity waves are absent, cannot be used to study such unstable flow, for inertial instability will rapidly destroy the balance. It has been proven that symmetric instability is the generator of quasi-2D meso- $\beta$ -scale systems. Linear theories point out that such instability is induced by the (amplifying) thermal wind imbalance of perturbations to the thermal wind balance satisfied by the (initial) basic flow.

## 6. Summary

Studies of the dynamics of torrential rainfall conducted by Chinese meteorologists in the last decade have focused on the following areas:

(1) A new potential temperature, the GMPT ( $\theta^*$ ) was invented, and the improved moist ageostrophic  $\mathbf{Q}$  vector ( $\mathbf{Q}_{um}$ ) for a non-uniformly saturated atmosphere was devised and evaluated in case studies of heavy rain.  $\mathbf{Q}_{um}$  has the advantage that its divergence  $\nabla \cdot \mathbf{Q}_{um}$  is a good indicator for making accurate 6-hour precipitation forecasts when, as is usually the case in the atmosphere (if not in earlier theories), the air is not uniformly saturated. Using  $\theta^*$ , the GMPV was introduced. This shows stronger signals and greater effectiveness

in diagnosing and analyzing rainfall events than traditional ones.

(2) SVD was proposed for both dry and saturated atmospheres.

(3) PV has limitations when applied to tropical deep convection. The newly-devised “convective vorticity vector” (CVV) proved very useful; the vertical component of the CVV is a strong signal closely related to deep convection development, a good tool for recognizing tropical convection.

(4) Mechanisms of frontogenesis have been intensively studied. In geostrophic adjustment frontogenesis, the initial temperature gradient can greatly influence cold front evolution. A suitable vapor distribution favors cold frontogenesis, and orographic forcing strengthens frontogenesis. Another study showed that boundary-layer friction plays a dual role in frontogenesis: frictional dissipation slows front development, while simultaneously enhancing ageostrophic flow, which promotes frontogenesis.

(5) The propagation of spiral rainbands and the development of dynamical instability in tropical cyclones have been explained by mixed wave-vortex dynamics.

(6) Wave-activity laws have extended the theory of wave–basic flow interaction from large-scale fields to mesoscale fields, generalized to include both rapid gravity-wave dynamics and the powerful effects of moisture and precipitation.

Since the dynamics of torrential rainfall is far from perfect, we still have much left to explore. With the collective effort of all Chinese meteorologists, the powerful economic support of the country and the science and technology boom in China, we believe that torrential rainfall research has a future that will be both intellectually and scientifically fruitful, as well as valuable to operational forecasting and the protection of lives and property from flooding and deluge.

**Acknowledgements.** This study was supported by the National Natural Science Foundation of China (Grant Nos. 91437215 and 41375052), State Key Laboratory of Severe Weather Open Project (Grant No. 2013LASW-A06), and the Key Research Program of the Chinese Academy of Sciences (Grant No. KZZD-EW-05-01). We thank J. P. BOYD for editorial assistance.

## REFERENCES

- Bennetts, D. A., and B. J. Hoskins, 1979: Conditional symmetric instability—A possible explanation for frontal rainbands. *Quart. J. Roy. Meteor. Soc.*, **105**, 945–962.
- Bergeron, T., 1928: Über die dreidimensionale verknüpfende Wetteranalyse. *I. Geof. Publ.*, **5**(6), 1–111. (in German)
- Bjerknes, J., 1918: Geofys. Publikasjoner, Norske Videnskaps-Akad, Oslo. **1**(2), 168 pp.
- Bleck, R., 1984: An isentropic coordinate model suitable for lee cyclogenesis simulation. *Rivista di Meteorologia Aeronautica*, **44**, 189–194.
- Blumen, W., and R. Wu, 1983: Baroclinic instability and frontogenesis with Ekman boundary layer dynamics incorporating the geostrophic momentum approximation. *J. Atmos. Sci.*, **40**, 2630–2637.
- Blumen, W., and R. Wu, 1995: Geostrophic adjustment and energy

- conversion. *J. Phys. Oceanogr.*, **25**, 428–438.
- Cui, X., S. Gao, and G. Wu, 2003: Up-sliding slantwise vorticity development and the complete vorticity equation with mass forcing. *Adv. Atmos. Sci.*, **20**(5), 825–836, doi: 10.1007/BF02915408.
- Davies-Jones, R., 1991: The frontogenetical forcing of secondary circulations. Part I: The duality and generalization of the Q vector. *J. Atmos. Sci.*, **48**(4), 497–509.
- Dunn, L. B., 1991: Evaluation of vertical motion: Past, Present, and Future. *Wea. Forecasting*, **6**, 65–73.
- Emanuel, K. A., 1983: The Lagrangian parcel dynamics of moist symmetric instability. *J. Atmos. Sci.*, **40**, 2368–2376.
- Fang, J., and R. Wu, 1998: Frontogenesis, evolution and the time scale of front formation. *Adv. Atmos. Sci.*, **15**(2), 233–246, doi: 10.1007/s00376-998-0042-4..
- Gao, S. T., and L. Ran, 2003: On the parameterization scheme of gravity wave drag effect on the mean zonal flow of mesosphere. *Chinese Science Bulletin*, **48**(10), 1020–1023.
- Gao, S. T., and L. K. Ran, 2009: Diagnosis of wave activity in a heavy-rainfall event. *J. Geophys. Res.*, **114**, D08119, doi: 10.1029/2008JD010172.
- Gao, S. T., T. Lei, and Y. S. Zhou, 2002: Moist potential vorticity anomaly with heat and mass forcing in torrential rain systems. *Chinese Physics Letters*, **19**(6), 878–880. (in Chinese)
- Gao, S. T., X. R. Wang, and Y. S. Zhou, 2004a: Generation of generalized moist potential vorticity in a frictionless and moist adiabatic flow. *Geophys. Res. Lett.*, **31**, L12113, doi: 10.1029/2003GL019152.
- Gao, S. T., F. Ping, X. F. Li, and W. K. Tao, 2004b: A convective vorticity vector associated with tropical convection: A two-dimensional cloud-resolving modeling study. *J. Geophys. Res.*, **109**, D14106, doi: 10.1029/2004JD004807.
- Gao, S. T., X. F. Li, W. K. Tao, C. L. Shie, and S. Lang, 2007: Convective and moist vorticity vectors associated with tropical oceanic convection: A three-dimensional cloud-resolving model simulation. *J. Geophys. Res.*, **112**, D01105, doi: 10.1029/2006JD007179.
- Gu, H. D., and Z. A. Qian, 1991: A discussion about the role of the water vapor source/sink term in continuity equation of numerical models. *Chinese Sci. Bull.*, **36**, 16–21.
- Gray, M. E. B., G. J. Shutts, and G. C. Craig, 1998: The role of mass transfer in describing the dynamics of mesoscale convective systems. *Quart. J. Roy. Meteor. Soc.*, **124**, 1183–1207.
- Haynes, P. H., 1988: Forced, dissipative generalizations of finite-amplitude wave activity conservation relations for zonal and nonzonal basic flows. *J. Atmos. Sci.*, **45**, 2352–2362.
- Hoskins, B. J., and F. P. Bretherton, 1972: Atmospheric frontogenesis models: Mathematical formulation and solution. *J. Atmos. Sci.*, **29**, 11–37.
- Hoskins, B. J., M. E. McIntyre, and A. W. Robertson. 1985: On the use and significance of isentropic potential vorticity maps. *Quart. J. Roy. Meteor. Soci.*, **111**, 877–946.
- Kleinschmidt, E., 1957: Dynamic meteorology. Vol. 48, *Handbuch der physik*, A. Eliassen and E. Kleinschmidt, Eds., 112–129.
- Lu, H. C., Z. Kou, J. F. Fei, X. L. Song, and K. Zhong, 2004: Some problems of unbalanced dynamics in the development of the mesoscale convective system. *Scientia Meteorologica Sinica*, **24**, 120–126. (in Chinese)
- Miller, J. E., 1948: On the concept of frontogenesis. *J. Meteor.*, **5**, 169–171.
- Newton, C. W., 1954: Frontogenesis and frontolysis as a three-dimensional process. *J. Atmos. Sci.*, **11**, 449–461.
- Ou, H. W., 1984: Geostrophic adjustment: A mechanism for frontogenesis. *J. Phys. Oceanogr.*, **14**, 994–1000.
- Pettersen, S., 1936: Contribution to the theory of frontogenesis. *Geophys. Publ.*, **11**(6), 1–27.
- Pettersen, S., 1956: *Weather Analysis and Forecasting*. Science Press, 32–40.
- Qiu, C. J., J. W. Bao, and Q. Xu, 1993: Is the mass sink due to precipitation negligible? *Mon. Wea. Rev.*, **121**, 853–857.
- Ran, L. K., and S. T. Gao, 2007: A three-dimensional wave-activity relation for pseudomomentum. *J. Atmos. Sci.*, **64**, 2126–2134.
- Reed, R. J., 1955: A study of a characteristic type of upper-level frontogenesis. *J. Atmos. Sci.*, **12**, 226–237.
- Reed, R. J., and E. F. Danilson, 1958: Fronts in the vicinity of the tropopause. *Arch. Much. Meteor. Geophys. Bioklim*, **A11**, 1–17.
- Schultz, D. M., and P. N. Schumacher, 1999: Review: The use and misuse of conditional symmetric instability. *Mon. Wea. Rev.*, **127**, 2709–2729.
- Scinocca, J. F. and T. G. Shepherd, 1992: Nonlinear wave-activity conservation laws and Hamiltonian structure for the two-dimensional anelastic equations. *J. Atmos. Sci.*, **49**, 5–27.
- Shaw, T. A., and T. G. Shepherd, 2008: Wave activity conservation laws for the three-dimensional anelastic and Boussinesq equations with a horizontally homogeneous background flow. *Journal of Fluid Mechanics*, **594**, 493–506.
- Shou, S. W., S. S. Li, and X. P. Yao., 2003: *Mesoscale Meteorology*. China Meteorological Press, 329 pp. (in Chinese)
- Tan, Z. M., and R. S. Wu, 2000a: A theoretical study of low-level frontal structure in the planetary boundary layer over orography. Part I: Cold front and uniform geostrophic flow. *Acta Meteorologica Sinica*, **58**, 137–150. (in Chinese)
- Tan, Z. M., and R. S. Wu, 2000b: A theoretical study of low-level frontal structure in the planetary boundary layer over orography. Part II: Warm front and uniform geostrophic flow. *Acta Meteorologica Sinica*, **58**, 265–277. (in Chinese)
- Tao, S., and Coauthor, 1980: *The Torrential Rain in China*. Science Press, Beijing, 225 pp. (in Chinese)
- Wang, X., and R. Wu, 1999: Interaction of orographic disturbance with front. *Adv. Atmos. Sci.*, **16**(3), 467–481, doi: 10.1007/s00376-999-0024-1.
- Wang, Y., R. Wu, and Y. Pan, 2000: Evolution and frontogenesis of an imbalanced flow—The influence of vapor distribution and orographic forcing. *Adv. Atmos. Sci.*, **17**(2), 256–274, doi: 10.1007/s00376-000-0008-7.
- Wu, G. X. and H. Z. Liu, 1997: Vertical vorticity development owing to down-sliding at slantwise isentropic surface. *Dyn. Atmos. Oceans*, **27**, 715–743.
- Wu, G. X., Y. P. Cai, and X. Q. Tang, 1995: Moist potential vorticity and slantwise vorticity development. *Acta Meteorologica Sinica*, **53**(3), 387–405. (in Chinese)
- Wu, R., and W. Blumen, 1982: An analysis of Ekman boundary layer dynamics incorporating the geostrophic momentum approximation. *J. Atmos. Sci.*, **39**, 1774–1782.
- Wu, R., and W. Blumen, 1995: Geostrophic adjustment of a zero potential vorticity flow initiated by mass and momentum imbalances. *J. Phys. Oceanogr.*, **25**, 439–445.
- Xu, Q., 1992: Ageostrophic pseudovorticity and geostrophic C-vector forcing—A new look at Q vector in three dimensions. *J. Atmos. Sci.*, **49**, 981–990.
- Yang, S., S. T. Gao, and D. H. Wang, 2007: Diagnostic analyses of the ageostrophic Q vector in the non-uniformly saturated,

- frictionless, and moist adiabatic flow. *J. Geophys. Res.*, **112**, D09114, doi: 10.1029/2006JD008142.
- Yao, X., Y. Yu, and S. Shou, 2004: Diagnostic analyses and application of the moist ageostrophic Q vector. *Adv. Atmos. Sci.*, **21**(1), 96–102, doi: 10.1007/BF02915683.
- Zhang, X. W., 1999: The expression of the modified Q vector and its application. *Journal of Tropical Meteorology*, **15**(2), 162–167. (in Chinese)
- Zhong, W., D. L. Zhang, and H. Lu, 2009: A theory for mixed vortex Rossby-Gravity waves in tropical cyclones. *J. Atmos. Sci.*, **66**, 3366–3381.
- Zhong, W., H. Lu, and D. L. Zhang, 2010: Mesoscale barotropic instability of vortex Rossby waves in tropical cyclones. *Adv. Atmos. Sci.*, **27**(2), 243–252, doi: 10.1007/s00376-009-8183-7.